Chemical Engineering Journal 154 (2009) 274–280

Contents lists available at ScienceDirect

Chemical Engineering Journal

journal homepage: www.elsevier.com/locate/cej

Hydrogen production from methanol over combustion-synthesized noble metal/ceria catalysts

George Avgouropoulos*, Joan Papavasiliou, Theophilos Ioannides

Foundation for Research and Technology-Hellas (FORTH), Institute of Chemical Engineering and High Temperature Chemical Processes (ICE-HT), P.O. Box 1414, GR-26504 Patras, Greece

ARTICLE INFO

Article history:
Received 5 December 2008
Received in revised form 11 February 2009
Accepted 11 March 2009

Keywords:
Hydrogen production
Methanol decomposition
Steam reforming
Noble metal
Ceria

ABSTRACT

Methanol decomposition (MD), steam reforming of methanol (SRM) and combined steam reforming of methanol (CSRM) were carried out over three noble metal (Pt, Pd, Rh)/ceria catalysts prepared via the combustion method. XPS measurements suggested the presence of highly dispersed (mainly) oxidized noble metal species in the as-prepared (oxidized) samples, while in-situ reduction led to metallic states only in the cases of palladium and platinum. Their activity increased in the order Rh < Pt < Pd for all three processes, while their selectivity towards CO production was remarkably high, even in the presence of steam, a fact that implies higher activity for methanol decomposition and lower activity for hydrolysis of methyl formate. Based on the activity/selectivity results an overall reaction scheme, which includes the production of both main products and by-products, is proposed.

1. Introduction

The production of H_2-rich gas streams for polymer electrolyte membrane fuel cells (PEMFCs) can be done in a fuel processor unit by reforming an alcohol or a hydrocarbon liquid fuel [1–3]. Alcohol fuels such as methanol have the benefits of a five to seven-fold higher energy density than compressed H_2, and at the same time are easily handled, stored and transported. In addition they are essentially sulphur-free and get reformed at moderate temperatures (200–300 °C) with low selectivity to byproducts (e.g. CO). Moreover, methanol can be produced from renewable sources (e.g. biomass), and as a consequence, may be considered as a sustainable energy carrier which would contribute to net-zero carbon dioxide (CO_2) emissions [3–5]. A challenge for fuel processing is the development of highly active and selective catalysts, which will be able to operate at temperatures as low as possible with minimal CO formation. H_2 production from methanol is possible through several catalytic routes [5–23]:

- methanol decomposition (MD)

$$CH_3OH = CO + 2H_2, \quad \Delta H^o = 92\,kJ\,mol^{-1} \tag{1}$$

- steam reforming of methanol (SRM)

$$CH_3OH + H_2O = CO_2 + 3H_2, \quad \Delta H^o = 49.4\,kJ\,mol^{-1} \tag{2}$$

- partial oxidation of methanol (POM)

$$CH_3OH + 1/2O_2 = CO_2 + 2H_2, \quad \Delta H^o = =192.2\,kJ\,mol^{-1} \tag{3}$$

- combined steam reforming of methanol (CSRM)

$$CH_3OH + (1-2\alpha)H_2O + \alpha O_2 = CO_2 + (3-2\alpha)H_2, (0 \le \alpha \le 0.5) \tag{4}$$

SRM is a process that provides a product gas with high H_2 content (up to 75%) and low CO concentration (1–2%). CO may be produced either as a primary product of direct MD reaction, or as a by-product via decomposition of various formates, such as methyl formate, or via the reverse water–gas shift reaction. Using O_2 together with steam CSRM offers advantages such as high reaction rates and thermo-balanced conditions.

Conventional copper-based SRM catalysts, such as $Cu/ZnO/Al_2O_3$, are pyrophoric if exposed to air and have poor thermal stability above 300 °C. Therefore, highly active and stable catalysts are required, mainly for mobile and portable fuel cell applications. Combustion-synthesized Cu–Ce and Cu–Mn oxide catalysts were recently found to be promising candidates for methanol reforming [5,10,13,19]. Noble metal-containing catalysts, especially Pt or Pd supported on reducible oxide supports, such ZnO and CeO_2, have been also proposed as an alternative to copper for the conversion of methanol to H_2 [23–32]. The Pd/Zn alloy formed at high reduction temperature is an active phase for the SRM reaction. On the other hand, CeO_2 is one of the most thermally stable oxides and under various redox conditions the oxidation state of the cation may vary between +3 and +4 [33]. Its distinct defect chemistry and the ability to exchange lattice

* Corresponding author. Tel.: +30 2610965272; fax: +30 2610965223.
E-mail address: geoavg@iceht.forth.gr (G. Avgouropoulos).

1385-8947/$ – see front matter © 2009 Elsevier B.V. All rights reserved.
doi:10.1016/j.cej.2009.03.019

oxygen with the gas phase results in an attractive oxide with unique catalytic properties, including the promotion of metal dispersion, the enhancement of the catalytic activity at the interfacial metal-support sites.

In the present work, the catalytic performance of three combustion-synthesized noble metal (Pt, Pd, Rh)/ceria catalysts has been investigated for the MD, SRM and CSRM processes. The physicochemical properties of as-prepared (oxidized) and in-situ reduced catalysts have been studied via BET, XRD, SEM and XPS techniques. A reaction scheme, which describes the possible pathways for the formation of hydrogen and by-products, is proposed.

2. Experimental

The urea-nitrate combustion method was used for the synthesis of Me/CeO_2 (Me = Pt, Pd, Rh) catalysts [34]. Nitrate salts of cerium [$Ce(NO_3)_3{\cdot}6H_2O$] and noble metal [$Pd(NO_3)_2$, $Rh(NO_3)_3$, $Pt(NH_3)_4(NO_3)_2$] were mixed with urea ($CO(NH_2)_2$) in an alumina crucible with the appropriate molar ratio (Me/(Me + Ce) = 0.0266, 75% excess of urea). The mixed solutions were preheated on a hot plate at ~80 °C to remove excess water. The resulting viscous gel was placed in an open muffle furnace, preheated at ~450 °C. The solution started boiling with frothing and foaming, and ignition took place after a few seconds –with rapid evolution of a large quantity of gases– yielding a voluminous solid product within a few minutes. In order to burn-off any carbonaceous residues, the powders were further heated at 550 °C for 1 h. All the produced powders were sieved to obtain the desired fraction ($90 < d_p < 180\ \mu m$). The samples were characterized by N_2 physisorption, XRD, SEM and XPS.

The specific surface area (S_{BET}), the pore volume (V_P) and the pore size distribution of the samples were determined from the adsorption and desorption isotherms of nitrogen at -196 °C using a Quantachrome Autosorb-1 instrument. Surface area was obtained following the BET (Brunauer–Emmett–Teller) procedure with six relative pressures of nitrogen in the range of 0.05–0.3. The pore size distribution was estimated using the BJH (Barrett, Joyner and Halenda) method. The total pore volume was determined at $P/P_0 = 0.995$. Prior to the measurements, the samples were outgassed at 200 °C for 2 h under vacuum.

The crystalline structure of the catalysts was analyzed with a X-ray powder diffractometer (Bruker D8 Advance) using Cu K_α radiation ($\lambda = 0.15418$ nm). The measurement was carried out in the 2θ angle range of 20–80°. The mean particle diameter of CeO_2 was calculated from the X-ray line broadening of the (1 1 1) diffraction peak according to Scherrer's equation [35].

The surface morphology of the catalytic samples with different Cu/(Cu + Ce) molar ratio was examined with a LEO SUPRA 35VP scanning electron microscope (SEM). Prior to SEM analysis the samples were placed on aluminum carbon paste-coated slabs, coated with a conductive layer of gold.

X-ray photoelectron spectra of CuO–CeO_2 catalysts were recorded with experiments that were carried out in a commercial ultrahigh vacuum system, equipped with a hemispherical electron energy analyzer (SPECS LH-10) and a twin anode X-ray gun for XPS measurements. The base pressure was 5×10^{-10} mbar. Unmonochromatized Al K_α line at 1486.6 eV and an analyzer pass energy of 97 eV were used in all XPS measurements. The XPS core level spectra were analyzed with a fitting routine which decomposes each spectrum into individual, mixed Gaussian–Lorentzian peaks using a Shirley background subtraction over the energy range of the fit. The binding energies were calculated by reference to the energy of C 1 s peak of contaminant carbon at 284.6 eV and the highest binding energy peak for Ce^{4+} $d_{3/2}$ at 916.5 eV. The surface composition of all samples in terms of atomic ratios was calculated, using empirical cross section factors for XPS [36].

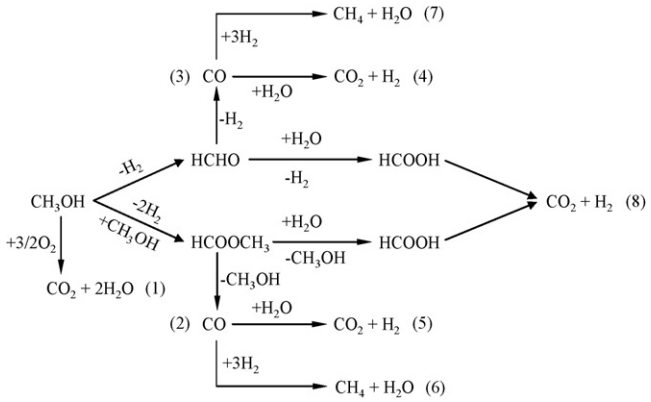

Scheme 1. Reaction pathways for the formation of primary products and by-products via MD, SRM and CSRM processes.

The catalytic performance for the MD, SRM and CSRM processes was investigated at atmospheric pressure, in the temperature range of 180–325 °C, in a fixed-bed reactor system, previously described [5,34]. The catalyst weight was 0.3 g and the total flow rate of the reaction mixture (MD: 5 vol.% CH_3OH/He; SRM: 5 vol.% CH_3OH/7.5% H_2O/He; CSRM: 5 vol.% CH_3OH/7.5% H_2O/0.5% O_2/He) was 70 $cm^3\ min^{-1}$ ($W/F = 0.257\ g\ s\ cm^{-3}$). The samples were pre-activated by exposure to the feed stream for 1 h at 300 °C, after which measurements were made by stepwise decrease of reaction temperature. Product and reactant analysis was carried out by a Shimadzu GC-14B equipped with TCD and FID.

Catalytic activity was evaluated in terms of methanol conversion. Hydrogen yield was calculated as the product of methanol conversion and H_2 selectivity. Selectivity to the carbon-containing product i was determined from:

$$Si = \frac{n_i C_i}{\sum n_i C_i} \tag{5}$$

where n_i is the number of carbon atoms in product i and C_i is the concentration of carbon-containing product i. If CO_2, $HCOOCH_3$, HCHO, CH_4 and CO were produced during via reaction pathways (2–7) in Scheme 1, then the selectivity of H_2 will be defined from the following equations:

$$MD: H_2\ \text{selectivity}\,(\%) = \frac{3C_{CO_2} + 2C_{CO} - C_{CH_4} + 2C_{HCOOCH_3} + C_{HCHO}}{2(C_{CO_2} + C_{CO} + C_{CH_4}) + 4C_{HCOOCH_3} + 2C_{HCHO}} \times 100 \tag{6}$$

$$SRM: H_2\ selectivity\,(\%) = \frac{3C + 2C_{CO} - C_{CH_4} + 2C_{HCOOCH_3} + C_{HCHO}}{3(C_{CO_2} + C_{CO} + C_{CH_4}) + 6C_{HCOOCH_3} + 3C_{HCHO}} \times 100 \tag{7}$$

$$CSRM: H_2 selectivity\,(\%) = \frac{3(C_{CO_2} - 0.333) + 2C_{CO} - C_{CH_4} + 2C_{HCOOCH_3} + C_{HCHO}}{3(C_{CO_2} - 0.333) + C_{CO} + C_{CH_4}) + 6C_{HCOOCH_3} + 3C_{HCHO}} \times 100 \tag{8}$$

The term "0.333" in Eq. (8) represents the amount of CO_2 which is produced from the combustion of methanol by co-fed oxygen:

$$\text{Methanol combustion}: CH_3OH + 3/2O_2 = CO_2 + 2H_2O \tag{9}$$

Table 1
Physical properties of noble metal/ceria catalysts.

Catalyst	S_{BET}, ($m^2\ g^{-1}$)	V_P, ($cm^3\ g^{-1}$)	$D_{CeO2(111)}$, (nm)
Pt/CeO_2	37.8	0.18	10.5
Pd/CeO_2	32.6	0.16	12.9
Rh/CeO_2	43.6	0.18	13.7

3. Results and discussion

The surface characteristics including the specific surface area (S_{BET}) and the total pore volume (V_P) of all noble metal/ceria catalysts, prepared with the combustion method, are presented in Table 1. For all samples, the isotherms of N_2 adsorption/desorption were of type II and had type B hysteresis loops, which closed at P/P_0 of ~0.40, as shown in Fig. 1A. The surface area (S_{BET}) of the catalysts increased in the order Pd < Pt < Rh and was in the range of 33–44 $m^2\ g^{-1}$. All the samples had broad pore size distributions (Fig. 1B), starting from ~4 nm and extending well into the macropore region. The pore volume of the samples was estimated to be in the range 0.16–0.18 $cm^3\ g^{-1}$.

Fig. 2 shows the XRD patterns of noble metal/ceria catalysts, as well as the pattern of pure CeO_2, prepared with the same technique, for comparison purposes. The fluorite oxide-type diffraction pattern of CeO_2 was observed in all samples. Crystallite sizes of cerium oxide, as calculated using Scherrer's equation, are reported in Table 1. No detectable diffractions of noble metals crystallites could be distinguished, suggesting that noble metals were highly dispersed. SEM micrographs (not shown) reflected the foamy and agglomerated nature of the material that has to do only with ceria, since it was impossible to detect any separate noble metal particles. The materials displayed a largely open porous structure with a lot of cracks and pores, which is associated with rapid evolution of gases during the combustion process. The particles were bound together into agglomerates and the nanosize nature of the combustion-derived materials was confirmed at higher magnifications of SEM.

X-ray photoelectron spectra of Pt 4f, Pd 3d and Rh 3d core level regions of Pt/CeO_2, Pd/CeO_2 and Rh/CeO_2, respectively, are shown in Fig. 3. The regional spectra were deconvoluted into sets of spin orbital doublets and the results are summarized in Table 2. Depending on the oxidation state of noble metal there are one (for rhodium, Fig. 3C), two (for palladium, Fig. 3B) or three (for platinum, Fig. 3A) sets of noble metal peaks. In the case of Pt/CeO_2 (as-prepared, oxidized form), Pt $4f_{7/2}$ peaks at 71.31, 72.78 and 74.22 eV suggest the presence of Pt^0, Pt^{2+} and Pt^{4+}, respectively [37–42]. The intensity of the corresponding metallic platinum peak is almost 50% of the total Pt 4f spectra in the oxidized sample. In-situ reduction at 300 °C under H_2 flow, led to increased amounts of reduced species. Indeed, the corresponding Pt^{4+} peak has disappeared and only Pt $4f_{7/2}$ peaks at 70.90 eV and 72.20 eV, assigned to Pt^0 and Pt^{2+} oxidation states, are observed in Fig. 3A. Accordingly, the intensity of the corresponding metallic platinum peak is increased to 81.3% with respect to the oxidized Pt/CeO_2 sample. A small amount of Pt^{2+} species after reduction may be related to incorporation of Pt^{2+} into the ceria lattice, which is difficult to reduce [39].

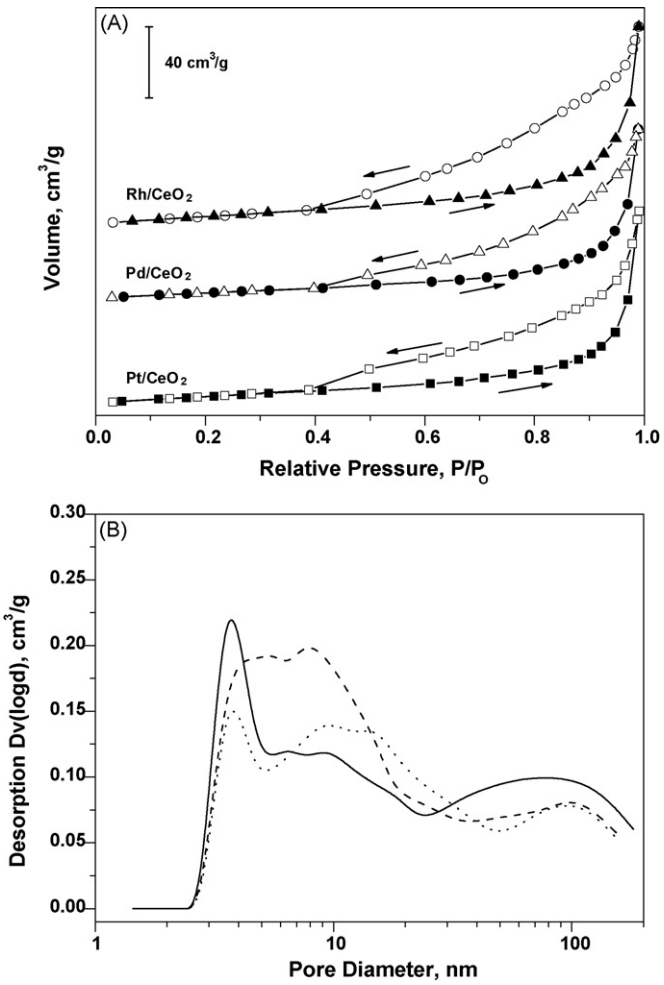

Fig. 1. (A) Adsorption/desorption isotherms of nitrogen at −196 °C and (B) pore size distribution (nitrogen desorption, BJH method) of Pt/CeO_2 (solid line), Pd/CeO_2 (dot line) and Rh/CeO_2 (dash line) catalysts.

Concerning Pd $3d_{5/2}$ peaks in Pd/CeO_2 catalyst (Fig. 3B), peaks at 336.55 eV and 338.62 eV can be attributed to PdO and Pd ions in CeO_2, respectively [23,40,41]. Palladium is in a highly ionic Pd^{2+} state, while corresponding metallic palladium peaks are missing. In-situ reduction at 300 °C under H_2 flow, led to complete reduction of palladium species, as shown by the exclusive appearance of Pd $3d_{5/2}$ peak at 335.01 eV.

Table 2
XPS analysis of noble metal/ceria catalysts.

Catalyst[a]	$Me/(Me+Ce)_{XPS}$	Binding energy of Pt $4f_{7/2}$, Pd $3d_{5/2}$ and Rh $3d_{5/2}$, (eV)	Species	Relative intensity, (%)	Ce^{4+}, (%)
Pt/CeO_2 (O)	0.161	71.31	Pt^0	48.1	97.1
		72.78	PtO, $Pt(OH)_2$	42.0	
		74.22	PtO_2	9.9	
Pt/CeO_2 (R)	0.113	70.90	Pt^0	81.3	77.1
		72.20	PtO, $Pt(OH)_2$	18.7	
Pd/CeO_2 (O)	0.124	336.55	PdO	70.0	96.4
		338.62	Pd in CeO_2	30.0	
Pd/CeO_2 (R)	0.081	335.01	Pd^0	100.0	94.3
Rh/CeO_2 (O)	0.177	308.90	Rh_2O_3	100.0	90.0
Rh/CeO_2 (R)	0.235	308.76	Rh_2O_3	100.0	75.7

[a] (O): oxidized, (R): in-situ reduction, 300 °C, 2 h, under H_2 flow. Nominal ratio: Me/(Me + Ce) = 0.0266.

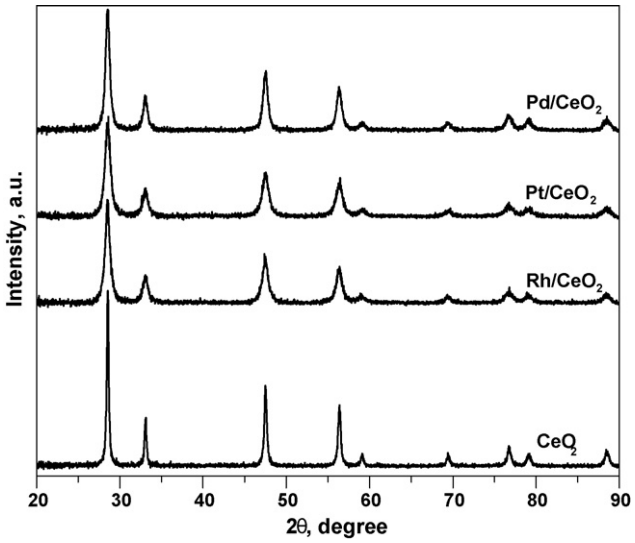

Fig. 2. XRD patterns of noble metal/ceria catalysts.

Fig. 3C presents the Rh 3d core level region of oxidized and reduced Rh/CeO_2 catalyst. The peak at the lower binding energy side (303.3 eV and 335.0 eV) in both spectra is due to the Ce (M_3VV) Auger line. Rh $3d_{5/2}$ peaks at 308.9 (oxidized sample) and 308.76 eV (reduced sample) suggest the presence of rhodium in the +3 oxidation state [43], despite the reduction treatment. The Ce 3d spectra (not shown) for the three catalysts with satellite features correspond to CeO_2 with Ce in the 4+ oxidation state. No variations in the Ce 3d spectra are seen in the three catalytic samples, and Ce $3d_{5/2}$ peak is centered at about 882.4 eV [24,34,37,38,41–43]. However, information about partial reduction of CeO_2 can be obtained from the intensity of the highest binding energy satellite for Ce^{4+} $d_{3/2}$ at 916.5 eV (μ'''satellite peak) [24]. The percentage of Ce^{4+} could be estimated by the equation $Ce^{4+} = \mu'''/14$, where $\mu'''$is the percentage of μ'''peak area with respect to the total Ce 3d area. The estimated values of Ce^{4+} are given in Table 2. A remarkable decrease in the relative concentration of Ce^{4+} species is observed in the case of Pt/CeO_2 and Rh/CeO_2 catalysts, while the percentage of Ce^{4+} slightly decreased in the case of reduced Pd/CeO_2 catalyst.

The surface concentration, represented as Me/(Me + Ce) atomic ratio, was estimated by XPS, and is presented in Table 2. The surface concentration of all noble metals is about 3–9 times higher than their nominal concentrations. Observation of Pt in the +2 and +4 states and 16.1% surface concentration, Pd in +2 state and 11.3% surface concentration, and Rh in +3 state and 17.7% surface concentration suggest that almost all the noble metal ions are highly dispersed on the ceria surface [37–43]. However, the formation of interfacial solid solutions due to incorporation of part of noble metal ions in ceria lattice cannot be excluded. The noble metal-ceria interface, where interfacial noble metal sites are located and the noble metal-Ce interaction takes place, appears to be important for catalytic activity, because of the transfer of electrons from the metal oxide to the noble metal, and as a consequence the effective activation energy for the formation of oxygen vacancies is lowered [40]. The maximum surface enrichment is observed with the rhodium catalyst, followed by the platinum catalyst. Reduction of the samples led to decrease of noble metal surface concentration in the case of platinum and palladium catalysts, probably due to migration of cerium on the surface of noble metal or/and agglomeration of surface species during formation of metallic crystallites, while surface enrichment was further enhanced in the case of rhodium catalyst.

The catalytic activity and selectivity of noble metal/ceria catalysts for the MD, SRM and CSRM processes are shown in Fig. 4A, 4B and C, respectively. These results are also summarized in Table 3. Methanol was selectively decomposed to CO and H_2 at low temperatures (<300 °C). The Pd/CeO_2 catalyst appeared to be the most active and selective among three catalysts examined for the MD process (Fig. 4A). The activity increased in the order Rh < Pt < Pd and the major products of the reaction were H_2 and CO, while the by-products were (i) CH_4, CO_2, H_2O, $HCOOCH_3$ and HCHO in most cases

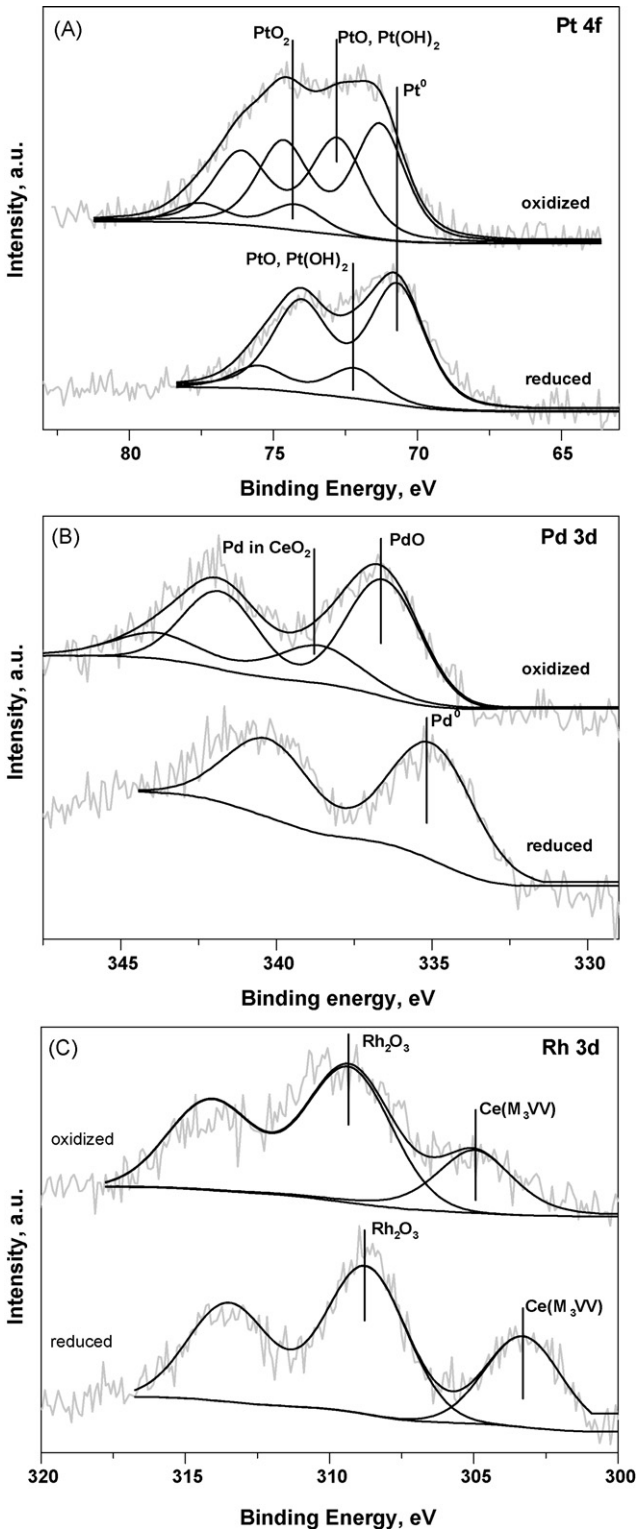

Fig. 3. XPS of Pt 4f (A), Pd 3d (B) and Rh 3d (C) core level regions of noble metal/ceria catalysts.

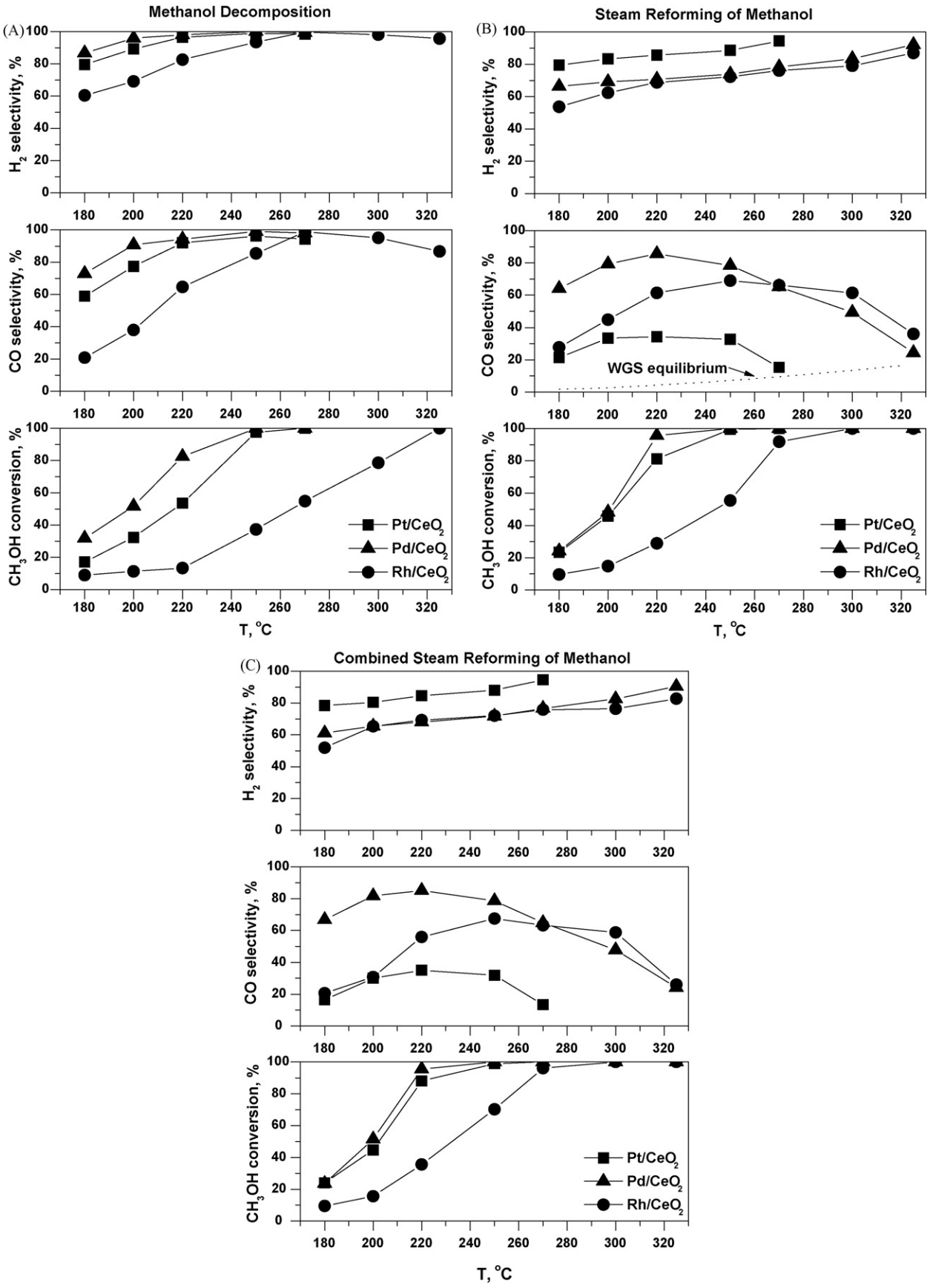

Fig. 4. Activity and selectivity for MD (A), SRM (B) and CSRM (C) processes over Pt/CeO_2 (■), Pd/CeO_2 (▲), and Rh/CeO_2 (●) catalysts.

Table 3
Activity and selectivity for MD, SRM and CSRM reactions over noble metal/ceria catalysts.

Reaction	MD				SRM				CSRM			
$T_{reaction}$ (°C)	200	220	250	270	200	220	250	270	200	220	250	270
Pt/CeO_2												
CH_3OH conversion (%)	32.4	53.6	97.5	100.0	45.8	81.2	99.5	100.0	44.7	88.0	98.9	100.0
H_2 yield (%)	28.9	51.7	96.4	98.5	38.2	69.5	88.2	94.4	36.0	74.5	87.0	94.6
C-product selectivity (%)												
CO_2	0.7	0.8	2.4	3.5	58.4	61.4	66.9	84.3	60.0	61.5	67.8	86.1
CO	77.4	92.0	96.1	94.3	33.4	34.3	32.8	15.4	30.0	35.1	31.9	13.5
CH_4	0.2	0.4	1.5	2.2	0.1	0.2	0.3	0.3	0.1	0.2	0.3	0.4
$HCOOCH_3$	21.7	6.8	0.0	0.0	7.6	3.9	0.0	0.0	9.3	3.0	0.0	0.0
HCHO	0.0[a]	0.0[a]	0.0	0.0	0.5	0.2	0.0	0.0	0.6	0.2	0.0	0.0
Pd/CeO_2												
CH_3OH conversion (%)	51.8	91.2	100.0	100.0	48.3	95.7	100.0	100.0	51.5	95.6	100.0	100.0
H_2 yield (%)	49.7	89.0	100.0	99.4	33.4	67.6	73.9	78.2	33.7	65.1	71.7	76.6
C-product selectivity (%)												
CO_2	0.5	0.5	0.8	1.0	14.0	13.2	21.6	34.8	14.0	13.1	21.3	35.0
CO	90.7	94.3	99.1	98.2	79.3	85.6	78.4	65.2	81.7	85.2	78.7	65.0
CH_4	0.0	0.0[a]	0.1	0.8	0.0	0.0	0.0	0.0[a]	0.0	0.0	0.0	0.0[a]
$HCOOCH_3$	8.8	5.2	0.0	0.0	6.4	1.2	0.0	0.0	4.1	1.6	0.0	0.0
HCHO	0.0	0.0	0.0	0.0	0.3	0.0[a]	0.0	0.0	0.2	0.0[a]	0.0	0.0
Rh/CeO_2												
CH_3OH conversion (%)	11.3	13.4	37.2	54.8	14.8	28.9	55.4	91.8	15.6	35.6	70.2	96.0
H_2 yield (%)	7.8	11.1	34.7	54.5	9.2	19.9	40.0	69.9	10.2	24.7	50.5	72.8
C-product selectivity (%)[b]												
CO_2	0.2	0.3	0.9	1.0	21.3	22.4	23.8	31.1	49.0	33.9	28.4	35.2
CO	37.9	64.6	85.5	98.2	44.8	61.4	69.1	66.1	30.9	56.0	67.5	63.3
CH_4	0.0	0.0	0.1	0.3	0.0	0.0[a]	0.0[a]	0.0[a]	0.0	0.0[a]	0.1	0.4
$HCOOCH_3$	61.9	35.1	13.5	0.0	31.8	15.3	6.6	2.6	18.8	9.6	3.8	1.0
HCHO	0.0	0.0	0.0	0.0	2.1	0.9	0.5	0.1	1.3	0.5	0.2	0.1

[a] Selectivities lower than 0.05%.
[b] Ethylene, ethane and propylene were identified at 270 °C, with selectivities lower than 0.5%.

and (ii) ethylene, ethane and propylene, formed only over Rh/CeO_2, at T≥270 °C with selectivities lower than 0.5%. The H_2 yield and CO selectivity increase with temperature increase and methanation (pathway (6) or (7) in Scheme 1) took place, while CO_2 was produced simultaneously. CO_2 might be formed by the water–gas shift (pathway (4) or (5) in Scheme 1) and/or methanol steam reforming (pathway (8) in Scheme 1) reactions. Required water for the formation of CO_2 was available by the methanation reaction. However, the selectivity of CO_2 is always higher than methane selectivity, a fact that might be attributed to: (i) oxygen trace impurities in the feed, (ii) the Boudouard reaction (6), (iii) oxygen supply from ceria support [27]. The latter process has a transient character and is not expected to be important under long-term operation. $HCOOCH_3$ selectivity decreased with temperature increase, accompanied by CO_2 formation increase, a fact that implies CO_2 formation via reaction pathway (5) or/and (4), since traces of HCHO formed at low temperatures over platinum catalysts vanish at higher temperatures.

On the other hand, in SRM process over noble metal/ceria catalysts (Fig. 4B and Table 3), the presence of water enhanced the catalytic activity of all the samples examined, while the selectivity towards $HCOOCH_3$ and CH_4 formation was diminished. The latter behavior was accompanied by increased selectivities towards HCHO formation. HCHO was not observed in MD process in almost all the cases, which suggests that the rate of dehydrogenation is much faster than the formation rate of HCHO (pathway (3) in Scheme 1). In the presence of steam, HCHO is attached by water to form HCOOH, and finally transformed to CO_2 and H_2O (pathway (8) in Scheme 1). Palladium catalyst remained the most active one, but not the most selective one, since the H_2 yield and selectivity towards CO_2 production were less than 80% and 35%, respectively, at the temperature where maximum CH_3OH conversion was obtained (i.e. 250–270 °C). The corresponding CO selectivity was higher than 65% at the same temperature range. Rhodium catalyst was less active than Pd/CeO_2 catalyst and showed similar behavior concerning H_2, CO_2 and CO selectivities. On the other hand, complete CH_3OH conversion was achieved over Pt/CeO_2 catalyst at 270 °C, with 94.4% H_2 selectivity, 84.3% CO_2 selectivity and 15.3% CO selectivity. The observed peak in CO selectivity curve (Fig. 4B) is related with the $HCOOCH_3$ concentration trend with temperature. Indeed, at low temperatures where $HCOOCH_3$ concentration is relative high, the corresponding CO concentration is relative low and increases with temperature increase and $HCOOCH_3$ concentration decrease. Further increase of temperature resulted in CO selectivity decrease due to the WGS reaction (pathways (4) and/or (5) in Scheme 1). The latter result is more obvious in Fig. 4B, where CO selectivity is remarkably higher than WGS equilibrium, and approaches it in the high temperature region. Among three catalysts examined, Pt/CeO_2 is the most active for WGS reaction [44], since its CO selectivity curve is much closer to the equilibrium line and approaches it at around 270 °C.

Under autothermal conditions (CSRM process, Fig. 4C and Table 3) the catalytic behavior followed the same trend in the case of Pt/CeO_2 and Pd/CeO_2 catalysts as in SRM, while the catalytic activity was improved only in the case of Rh/CeO_2 catalyst. The improved catalytic activity for methanol reforming by co-feeding oxygen along with steam and methanol has been attributed to more efficient heat transfer in the catalytic bed, because oxygen is initially consumed through combustion of part of methanol feed (pathway (1) in Scheme 1) and heat is generated in situ in the direction of flow [5,12,18].

In terms of H_2 yield and CO selectivity (Table 3), the following observations can be made: (a) rhodium was the least active catalyst for MD, SRM and CSRM reactions, (b) palladium was the most active and selective catalyst for MD process and (c) platinum catalyst gave the highest H_2 yields and lowest CO selectivities for SRM and CSRM reactions. In all cases, however, CO selectivity is considerably higher compared to the one obtained over Cu-based catalysts [5,10,12].

Based on the results of the present work and taking into account previous reports on methanol decomposition/reforming processes

over noble metal catalysts two parallel reaction pathways may be proposed (Scheme 1). The dissociation of the hydroxyl group from methanol takes place rapidly on the noble metal surface, while the breaking of the C-H bond in the adsorbed methoxy group CH_3O is considered as the rate-determining step [24,26,27]. The formation of relative high concentrations of $HCOOCH_3$ during MD process at temperatures lower than 250 °C, while only traces of HCHO are observed, implies that the reaction pathway (3) proceeds much faster than reaction pathway (2) at low temperatures. At higher temperatures, both reaction steps contribute equally to the production of CO. $HCOOCH_3$ selectivity follows the noble metal activity trend. Rhodium was the least active catalyst and at the same time the most selective towards $HCOOCH_3$ formation, a fact that might be attributed to lower activity for the hydrolysis of $HCOOCH_3$ (pathway (2) in Scheme 1). In the presence of water (SRM and CSRM processes) catalysts activity for the hydrolysis of $HCOOCH_3$ increases without changing the catalysts activity order. Palladium is the most efficient catalyst for methanol transformation and at the same time the least effective in the presence of H_2O, in the sense that MD is also taking place under SRM conditions. This may be attributed to weaker H_2O adsorption on Pd or relatively stronger CH_3OH adsorption compared to Rh or Pt. In the case of Pt and Rh catalysts, H_2O has a clearly positive effect on catalytic activity, which may be attributed to methyl formate hydrolysis. In addition Pt/CeO_2 is known to be an active WGS catalyst [44].

Ceria plays an important role in creation of additional sites at the interface, for methanol adsorption and production of methoxy and formate species, while the distinct defect chemistry of ceria and the ability to provide lattice oxygen might play a significant role via maintaining the noble metals in a more active cationic state. It has been reported that the presence of oxidized states of noble metals, favored in the present work by the combustion synthesis route and evidenced by XPS measurements, promotes the breaking of the C–H bond [24,27].

Combustion-synthesized noble metal/ceria catalysts examined in the present work are significantly more active than copper-based catalysts, prepared with the same method [17], in methanol decomposition, while their activity is comparable in the presence of steam [5,10,12,17,18]. However, noble metal catalysts show much higher selectivities towards CO production, even in the presence of steam, a fact that implies higher activity for methanol decomposition and lower activity for hydrolysis of $HCOOCH_3$, in contrast with copper-based catalysts [20,45].

4. Conclusions

Pt^0-, Pt^{2+}- and Pt^{4+}-like species were formed on the combustion-synthesized (oxidized) Pt/CeO_2 catalyst surface, while rhodium was dispersed on the +3 oxidation state on ceria and palladium was found to be in a highly ionic +2 state. In-situ reduction with H_2 at 300 °C led to metallic states only in the case of Pt (82% Pt^0, 18% Pt^{2+}) and Pd (100% Pd^0) catalysts. Significant enrichment (up to nine times with respect to the nominal loading) of the catalyst surface with noble metal species was observed in all three samples, indicating high noble metal dispersion. Methanol was selectively decomposed to CO and H_2 at low temperatures (<300 °C, MD process) on combustion-synthesized noble metal/ceria catalysts. Their activity increased in the order Rh < Pt < Pd. CH_4, CO_2, H_2O, $HCOOCH_3$ and HCHO were identified as main by-products of MD process in most cases. The presence of water (SRM and CSRM processes) enhanced the catalytic activity of all the samples examined, while the selectivity towards $HCOOCH_3$ and CH_4 formation was diminished. Two parallel reaction pathways were proposed for the formation of CO: formation of (a) formaldehyde and (b) methyl formate. However, noble metal catalysts showed high selectivities towards CO production, even in the presence of steam, a fact that implies higher activity for methanol decomposition and lower activity for hydrolysis of $HCOOCH_3$, in contrast with literature-proposed copper-based catalysts.

Acknowledgement

The work was carried out in the frame of a postdoctoral fellowship funded from the State Scholarship Foundation, Greece.

References

[1] A. Ghenciu, Curr. Opin. Solid State Mater. Sci. 6 (2002) 389.
[2] D.L. Trimm, Z.I. Önsan, Catal. Rev. 43 (2001) 31.
[3] A. Biyikoglu, Int. J. Hydrogen. Energy 30 (2005) 1181.
[4] N. Liu, Z. Yuan, C. Wang, L. Pan, S. Wang, S. Li, D. Li, S. Wang, Chem. Eng. J. 139 (2008) 56.
[5] J. Papavasiliou, G. Avgouropoulos, T. Ioannides, J. Catal. 251 (2007) 7.
[6] A. Basile, G.F. Tereschenko, N.V. Orekhova, M.M. Ermilova, F. Gallucci, A. Iulianelli, Int. J. Hydrogen Energy 31 (2006) 1615.
[7] A. Iulianelli, Int. J. Hydrogen Energy 31 (2006) 1615.
[8] J.-P. Shen, C. Song, Catal. Today 77 (2002) 89.
[9] S. Muscia-Mascarós, R.M. Navarro, L. Gómez-Sainero, U. Constantino, M. Ncchetti, L.G. Fierro, J. Catal. 198 (2001) 338.
[10] J. Papavasiliou, G. Avgouropoulos, T. Ioannides, Catal. Commun. 6 (2005) 497.
[11] C.J. Jiang, D.L. Trimm, M.S. Wainwright, N.W. Cant, Appl. Catal. A: Gen. 97 (1993) 145.
[12] J. Papavasiliou, G. Avgouropoulos, T. Ioannides, Catal. Commun. 5 (2004) 231.
[13] S. Velu, K. Suzuki, Top. Catal. 22 (2003) 235.
[14] B. Lindström, J. Agrell, L.J. Pettersson, Chem. Eng. J. 93 (2003) 91.
[15] S. Liu, K. Takahashi, K. Uematsu, M. Ayabe, Appl. Catal. A: Gen. 283 (2005) 125.
[16] M. Lyubovski, S. Roychoudhury, Appl. Catal. B: Environ. 54 (2004) 203.
[17] J. Papavasiliou, G. Avgouropoulos, T. Ioannides, Appl. Catal. B: Environ. 69 (2007) 226.
[18] J. Papavasiliou, G. Avgouropoulos, T. Ioannides, Appl. Catal. B: Environ. 66 (2006) 168.
[19] T. Valdés-Solís, G. Marbán, A.B. Fuertes, Catal. Today 116 (2006) 354.
[20] B. Frank, F.C. Jentoft, H. Soerijanto, J. Kröhnert, R. Schlögl, R. Schomäcker, J. Catal. 246 (2007) 177.
[21] X. Hong, S. Ren, Int. J. Hydrogen Energy 33 (2008) 700.
[22] B.A. Peppley, J.C. Amphlett, L.M. Kearns, R.F. Mann, Appl. Catal. A: Gen. 179 (1999) 31.
[23] N. Takezawa, N. Iwasa, Catal. Today 36 (1997) 45.
[24] K. Sun, W. Lu, M. Wang, X. Xu, Appl. Catal. A: Gen. 268 (2004) 107.
[25] Y. Suwa, S. Ito, S. Kameoka, K. Tomishige, K. Kunimori, Appl. Catal. A: Gen. 267 (2004) 9.
[26] S. Imamura, T. Higashihara, Y. Saito, H. Aritani, H. Kanai, Y. Matsumura, N. Tsuda, Catal. Today 50 (1999) 369.
[27] Y. Liu, T. Hayakawa, T. Ishii, M. Kumagai, H. Yasuda, K. Suzuki, S. Hamakawa, K. Murata, Appl. Catal. A: Gen. 210 (2001) 301.
[28] L.M. Gómez-Sainero, R.T. Baker, I.S. Metcalfe, M. Sahibzada, P. Concepción, J.M. López-Nieto, Appl. Catal. A: Gen. 294 (2005) 177.
[29] N. Iwasa, T. Mayanagi, W. Nomura, M. Arai, N. Takezawa, Appl. Catal. A: Gen. 248 (2003) 153.
[30] M.P. Kapoor, Y. Ichihashi, K. Kuraoka, Y. Matsumura, J. Mol. Catal. A: Chem. 198 (2003) 303.
[31] N. Iwasa, T. Mayanagi, N. Ogawa, K. Sakata, N. Takezawa, Catal. Lett. 54 (1998) 119.
[32] Y.H. Chin, R. Dagle, J.L. Hu, A.C. Dohnalkova, Y. Wang, Catal. Today 77 (2002) 79.
[33] A. Trovarelli, Catal. Rev. 38 (1996) 439.
[34] G. Avgouropoulos, T. Ioannides, Appl. Catal. A: Gen. 244 (2003) 155.
[35] H.P. Klug, L.E. Alexander, X-Ray Diffraction Procedures, 2nd ed., Wiley, New York, 1974, p. 642.
[36] D. Briggs, M.P. Seah, Practical Surface Analysis by Auger and X-ray Photoelectron Spectroscopy, Wiley, Chichester, 1983.
[37] M.A. Scibioh, S. Kim, E.A. Cho, T. Lim, S. Hong, H.Y. Ha, Appl. Catal. B: Environ. 84 (2008) 773.
[38] P. Bera, K.R. Priolkar, A. Gayen, P.R. Sarode, M.S. Hegde, S. Emura, R. Kumashiro, V. Jayaram, G.N. Subbanna, Chem. Mater. 15 (2003) 2049.
[39] P. Bera, A. Gayen, M.S. Hegde, N.P. Lalla, L. Spadaro, F. Frusteri, F. Arena, J. Phys. Chem. B 107 (2003) 6122.
[40] Y. Zhang, J. Zhou, Z. Wang, J. Liu, K. Cen, Int. J. Hydrogen Energy 33 (2008) 2211.
[41] P. Bera, K.C. Patil, V. Jayaram, G.N. Subbanna, M.S. Hegde, J. Catal. 196 (2000) 293.
[42] K.R. Priolkar, P. Bera, P.R. Sarode, M.S. Hegde, S. Emura, R. Kumashiro, N.P. Lalla, Chem. Mater. 14 (2002) 2120.
[43] A. Gayen, K.R. Priolkar, P.R. Sarode, V. Jayaram, M.S. Hegde, G.N. Subbanna, S. Emura, Chem. Mater. 16 (2004) 2317.
[44] P. Panagiotopoulou, J. Papavasiliou, G. Avgouropoulos, T. Ioannides, D. Kondarides, Chem. Eng. J. 134 (2007) 16.
[45] J. Papavasiliou, G. Avgouropoulos, T. Ioannides, Appl. Catal. B: Environ. doi:10.1016/j.apcatb.2008.10.018, in press.